## 21.4 A 0.2°/hr Micro-Gyroscope with Automatic CMOS Mode Matching

Ajit Sharma, M. Faisal Zaman, Farrokh Ayazi

Georgia Institute of Technology, Atlanta, GA

Micromachined gyroscopes constitute one of the fastest growing segments of the microsensor market. The application domain of these devices is quickly expanding from automotive to consumer and personal navigation systems. Examples include anti-skid and safety systems in cars, and image stabilization in digital cameras. Today, MEMS gyros do not meet the sub-degree-per-hour resolution and bias drift requirements needed in high precision applications such as inertial measurement units (IMU) for GPS augmented navigation, robotics, unmanned surveillance vehicles, aircraft and personal heading references. This paper presents an interface architecture and CMOS ASIC for substantially improving the performance of a high-Q tuning fork gyroscope (TFG) through automatic matching of its resonant modes, yielding a low-cost silicon microgyro with bias drift of 0.2°/hr – two orders of magnitude better than commercially available MEMS gyros [1] and the lowest recorded to date for a MEMS gyro.

Figure 21.4.1 shows the SEM view of an in-plane TFG [2] fabricated on a 60μm thick SOI substrate using a two-mask process similar to the one used for the micro-g accelerometers reported in [3]. The proof-masses are driven into resonant oscillations along the *x*-axis using comb-drive electrodes (drive mode), and the Coriolis acceleration induced by rotation about the *z*-axis is sensed capacitively along the *y*-axis (sense mode). A CMOS transimpedance (TZ) front-end with TZ gains up to 22MΩ, capacitive resolution of 0.003aF/√Hz and 104dB SNDR was used for sensing the Coriolis rotation [4]. Quadrature nulling and automatic matching of drive and sense mode frequencies are still required, however, to ensure maximum sensitivity. This paper presents a 6mW CMOS IC interfaced with a control algorithm that adaptively biases the mechanical structure such that the drive and sense mode frequencies are equalized. This allows us to leverage the inherently high quality factor of the TFG and obtain an angular rate sensor with superior sensitivity and bias drift. The complete microsystem is shown in Fig. 21.4.2.

The sense mode is designed to be slightly higher in frequency than the drive mode to enable mode-matching even in the presence of process variations. Mode-matching is achieved by increasing the DC polarization voltage ($V_P$) on the MEMS structure until electrostatic spring softening decreases the sense mode frequency to become equal to that of the drive mode (0Hz split). This feature differentiates the mode-matched tuning fork gyroscope (M²-TFG) from other MEMS gyros [1]. Earlier approaches to mode-matching [2,4,5] involved measurements of the frequency responses and manual adjustments of $V_P$. These adjustments are time intensive and impractical to incorporate into an IMU. In addition, environmental effects such as vibration, mechanical shock and aging can cause the modes to mismatch by a few hertz in operation, which in turn affects sensor scale factor and bias stability. The presented mode-matching scheme exploits the unique characteristics of the sensor to achieve and maintain a zero or finite frequency split between the two modes in a fraction of the time and hardware required by the scheme presented in [5].

Quadrature error arises because of off-axis motion of the proof-masses caused by fabrication induced device misalignments, and results in unwanted zero rate output (ZRO) at the sensor operating frequency. The ZRO is minimized in a post fabrication trimming step by applying DC voltages at specific quadrature nulling electrodes (Fig. 21.4.1) to properly align the device. Despite quadrature nulling, there always exists a finite amount of ZRO. The amplitude of this residual ZRO is maximized when the modes are matched and can therefore be used as an indicator of sensor sensitivity. Once matched, synchronous I-Q demodulation [4] is used to distinguish between the quadrature error and the Coriolis signal.

The main blocks of the automatic mode-matching system are shown in Fig. 21.4.3. The ZRO level is detected using an envelope detector consisting of a $g_m$-cell followed by a full-wave rectifier and integrator. The full-wave rectifier uses a "floating" battery bias [6] and the detector has 6.5b linearity between 200mV$_{PP}$ and 1.2V$_{PP}$. The DC level is converted to a bit-stream using a 1st-order ΔΣ modulator, read into the PC via GPIB and decimated using MATLAB. The integrator in the ΔΣ modulator uses a noise optimized single-ended two-stage OTA [3] and correlated double sampling to mitigate flicker noise and offset. The power dissipation is 0.9mW at a clock frequency of 25.6kHz and the measured peak SNR for a signal of 100Hz is 86dB/Hz.

The mode-matching algorithm has been implemented in MATLAB and performs three steps in each iteration until a maximum in ZRO level is detected: (1) it sends an interrupt (START) to the timing unit that generates digital pulses which read in the ADC bit stream, resets the level detector and updates the counter values; (2) it compares the decimated value of the ZRO level from the current iteration with that from the previous one; and (3) it outputs a 2b control word to the $V_P$ stepper. Once the maximum has been detected, $V_P$ is decremented to its previous value, which corresponded to peak sensitivity. A timing diagram is shown in Fig. 21.4.3. Finally, at matched-mode, the distinct 90° phase difference that exists between the drive signal (0°drv) and the ZRO is monitored to ensure that mode-matching has indeed been achieved.

The $V_P$ stepper consists of an 8b up-down counter and a DAC implemented using a 6 + 3 partially-segmented current-steering architecture [7]. Since area was a constraint, the unary current source array was split only in two, resulting in INL of 0.92 LSB for a full-scale current of 8μA. The up/down counter counts up, down, or holds the value based on the 2b control word. Finally an XOR phase detector is used to monitor the phase difference between the drive and sense signals. The comparators ensure that the phase detector output is purely indicative of phase change and any amplitude variations are ignored.

Figure 21.4.4 shows the results of interfacing the M²-TFG with the mode-matching ASIC. The upper graph shows the ZRO output increasing as the DAC is incremented (lower trace). Once the maximum has been reached, the ZRO level does not increase further and the DAC decrements to its previous value. The inset shows the 90° phase difference that exists between the drive signal and ZRO in a matched mode condition. One particular advantage of the proposed scheme is that once matched, the modes can be mismatched by a known amount in a controlled fashion using the up/down counter to obtain a desired bandwidth. Secondly, the scheme is generic and can be applied to other gyroscopes [8]. An Allan variance analysis was used to characterize the superior long-term stability of the matched-mode device. Figure 21.4.5 illustrates the root-Allan variance plot for this device showing a bias stability of 0.2°/hr, without applying any pre-whitening or filtering. The maximum rate sensitivity was 88mV/°/s. Also shown in the figure is the final matched-mode frequency response of the device. Figure 21.4.6 summarizes the key parameters of the sensor and the IC. Figure 21.4.7 shows the die micrograph of the 6mW, 2.25mm² mode-matching ASIC fabricated in 0.6μm CMOS.

*Acknowledgements:*
This work was sponsored by the DARPA HERMIT program and the Georgia Tech Analog Consortium (GTAC). The authors would like to thank Dr. B. V. Amini for helpful discussions, Georgia Tech Microelectronics Research Center staff for their support and the MOSIS Educational Partnership (MEP) for IC fabrication.

*References*

[1] J. Geen et al., "Single-Chip Surface Micromachined Integrated Gyroscope with 50°/h Allan Deviation," *IEEE J. Solid-State Circuits*, pp. 1860-1866, Dec., 2002.
[2] M.F. Zaman, A. Sharma and F. Ayazi, "High Performance Matched-Mode Tuning Fork Gyroscope," *19th IEEE Int'l Conf. MEMS*, pp. 66-69, Jan., 2006.
[3] B. V. Amini and F. Ayazi, "A 2.5-V 14-bit ΔΣ CMOS-SOI Capacitive Accelerometer," *IEEE J. Solid-State Circuits*, pp. 2467-2476, Dec., 2004.
[4] A. Sharma, M. F. Zaman and F. Ayazi, "A 104dB SNDR Transimpedance based CMOS ASIC for Tuning Fork Microgyroscopes," *Proc. CICC,* pp. 655-658, Sept., 2006.
[5] D. Keymeulen et al., "Evolutionary Computation Applied to the Tuning of MEMS Gyroscopes," *Proc. GECCO 2005*, Vol. 1, pp. 927-935, June, 2005.
[6] S. Zhak et al., "A Low-Power Wide Dynamic Range Envelope Detector," *IEEE J. Solid-State Circuits*, pp. 1750-1753, Oct., 2003.
[7] J. Bastos, et al., "A 12-Bit Intrinsic Accuracy High-Speed CMOS DAC," *IEEE J. Solid-State Circuits*, pp. 1959-1969, Dec., 1998.
[8] M.F. Zaman, A. Sharma and F. Ayazi, "The Resonating Star Gyroscope," *18th IEEE Int'l Conf. MEMS*, pp. 355-358, Jan., 2005.

 

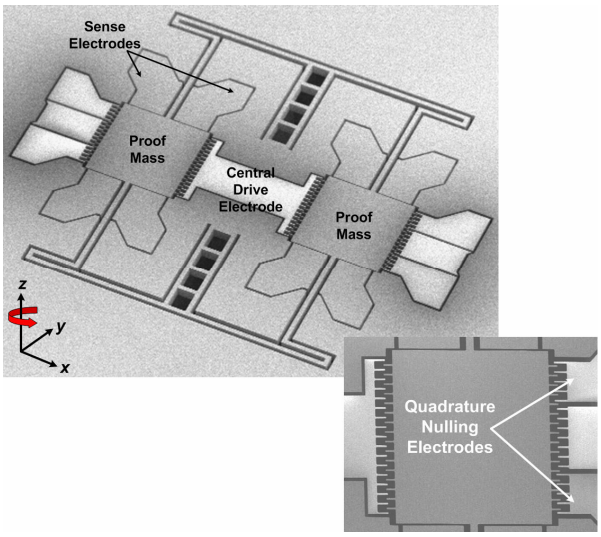


Figure 21.4.1: SEM view of the M²-TFG and close-up showing quadrature nulling electrodes.

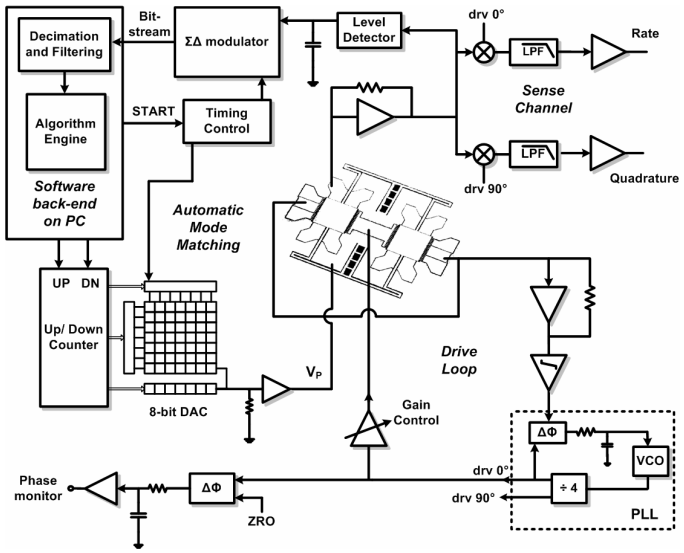


Figure 21.4.2: Block diagram of the entire microgyroscope system.

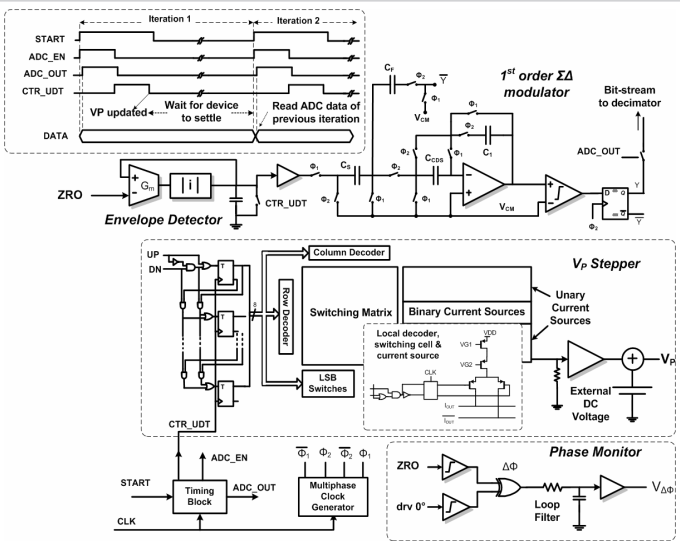


Figure 21.4.3: Schematic of the automatic mode-matching circuit and timing diagram of algorithm iterations (inset).

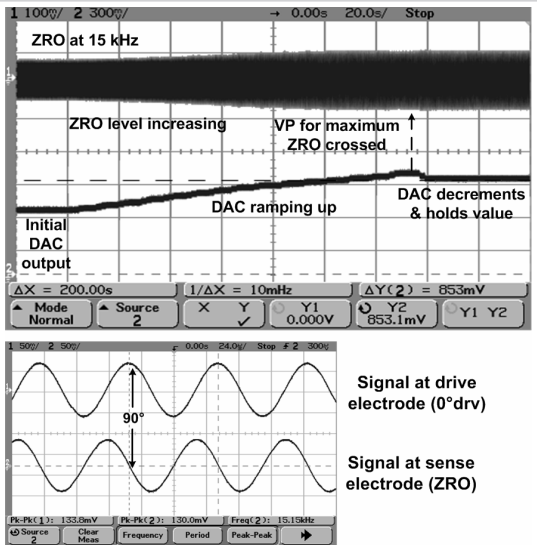


Figure 21.4.4: Automatic mode-matching output and 90°phase difference between 0°drv signal and ZRO (inset).

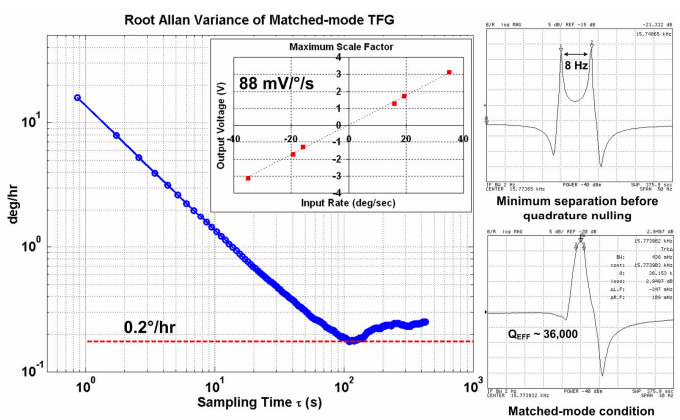


Figure 21.4.5: Root-Allan variance, scale factor and frequency response of the M²-TFG.

| Mode-matched Tuning Fork Gyroscope Performance | |
|---|---|
| Micro-Gyroscope area | 1mm x 1mm |
| Sensor Brownian noise floor | 0.18 °/hr/rt(Hz) |
| Sensor + Electronics bias stability | 0.2 °/hr |
| Matched-mode quality factor | 36,000 |
| Capacitive sensitivity of gyro | 300 aF/°/s |
| Minimum detectable ΔC | 0.003 – 3 aF/rt(Hz) |
| DAC INL (8-bits resolution) | 0.92 LSB |
| Maximum ΣΔ SNR ($f_{CLK}$ = 25.6 kHz) | 86dB (13 bits) |
| Stability of DAC output over time (4 hrs) | 0.1% |
| Maximum rate sensitivity of gyroscope | 88mV/°/s |
| IC die area (0.6 µm CMOS) | 2.25 mm² |
| Total power consumption | 6 mW (±1.5 V) |

Figure 21.4.6: Measured performance of the M²-TFG and mode-matching IC.

Continued on Page 610

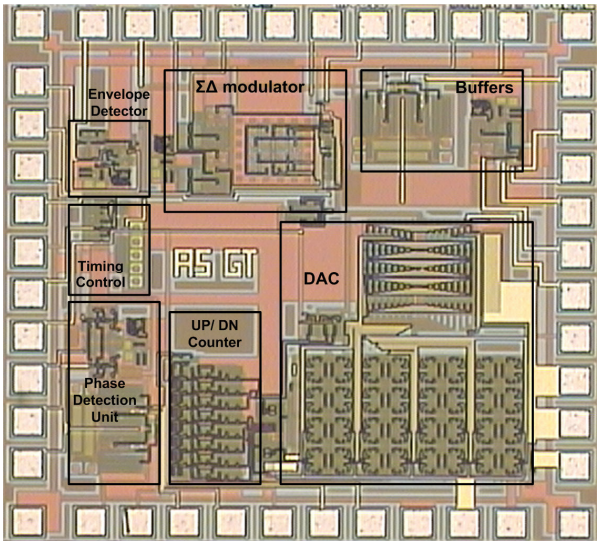


Figure 21.4.7: Die micrograph.

 